PAPER

Non-injective gas sensor arrays: identifying undetectable composition changes

To cite this article: Nickolas Gantzler et al 2021 J. Phys.: Condens. Matter 33 464003

View the article online for updates and enhancements.

You may also like

- An auditory brain-computer interface evoked by natural speech M A Lopez-Gordo, E Fernandez, S Romero et al.
- Altered inter-frequency dynamics of brain networks in disorder of consciousness Lihui Cai, Jiang Wang, Yao Guo et al.
- <u>Universities: Recession inhibits Japan's industrial input</u>
 Frederick Shaw Myers



IOP ebooks™

Bringing together innovative digital publishing with leading authors from the global scientific community.

Start exploring the collection-download the first chapter of every title for free.

J. Phys.: Condens. Matter 33 (2021) 464003 (16pp)

https://doi.org/10.1088/1361-648X/ac1e49

Non-injective gas sensor arrays: identifying undetectable composition changes

Nickolas Gantzler^{1,5}, E Adrian Henle^{2,5}, Praveen K Thallapally³, Xiaoli Z Fern⁴ and Cory M Simon^{2,*}

- ¹ Department of Physics, Oregon State University, Corvallis, OR, United States of America
- ² School of Chemical, Biological, and Environmental Engineering, Oregon State University, Corvallis, OR, United States of America
- ³ Pacific Northwest National Laboratory, Richland, WA, United States of America
- ⁴ School of Electrical Engineering and Computer Science, Oregon State University, Corvallis, OR, United States of America

E-mail: cory.simon@oregonstate.edu

Received 16 June 2021, revised 12 August 2021 Accepted for publication 17 August 2021 Published 7 September 2021



Abstract

Metal-organic frameworks (MOFs) are nanoporous materials with good prospects as recognition elements for gas sensors owing to their adsorptive sensitivity and selectivity. A gravimetric, MOF-based sensor functions by measuring the mass of gas adsorbed in a MOF. Changes in the gas composition are expected to produce detectable changes in the mass of gas adsorbed in the MOF. In practical settings, multiple components of the gas adsorb into the MOF and contribute to the sensor response. As a result, there are typically many distinct gas compositions that produce the same single-sensor response. The response vector of a gas sensor array places multiple constraints on the gas composition. Still, if the number of degrees of freedom in the gas composition is greater than the number of MOFs in the sensor array, the map from gas compositions to response vectors will be non-injective (many-to-one). Here, we outline a mathematical method to determine undetectable changes in gas composition to which non-injective gas sensor arrays are unresponsive. This is important for understanding their limitations and vulnerabilities. We focus on gravimetric, MOF-based gas sensor arrays. Our method relies on a mixed-gas adsorption model in the MOFs comprising the sensor array, which gives the mass of gas adsorbed in each MOF as a function of the gas composition. The singular value decomposition of the Jacobian matrix of the adsorption model uncovers (i) the unresponsive directions and (ii) the responsive directions, ranked by sensitivity, in gas composition space. We illustrate the identification of unresponsive subspaces and ranked responsive directions for gas sensor arrays based on Co-MOF-74 and HKUST-1 aimed at quantitative sensing of CH₄/N₂/CO₂/C₂H₆ mixtures relevant to natural gas sensing.

Keywords: gas sensor arrays, gas sensors, MOFs, electronic nose

(Some figures may appear in colour only in the online journal)

1. Introduction

Gas sensors [1] have a wide range of applications in the chemical industry and in emerging domains such as air quality monitoring [2], diagnosis of disease [3], food quality

assessment [4], detection of chemical warfare agents and explosives [5, 6], and crop monitoring [7].

Metal-organic frameworks (MOFs) [8] are nanoporous materials with high prospects as recognition elements for enhanced gas sensors [9–12] owing to their adsorptive sensitivity and selectivity. More, many MOFs exhibit chemical, thermal, and mechanical stability, making them suitable for sensing in practical conditions [13, 14]. MOFs offer large

^{*} Author to whom any correspondence should be addressed.

⁵ Equal contribution.

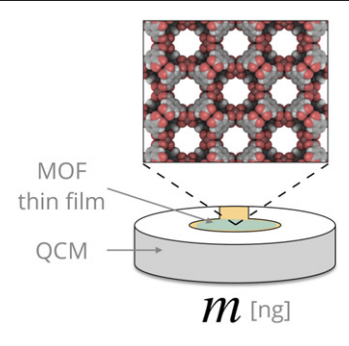


Figure 1. A gravimetric sensor comprised of a thin film of MOF [25] (the recognition element), in this case HKUST-1 [37], mounted on a QCM [24, 38] (the signal transducer). The QCM measures the (total) adsorbed mass of gas, m, in the thin film of MOF. The QCM-MOF functions as a sensor because changes in the gas composition are expected to cause changes in m.

internal surface areas and, often, expose functional groups and open metal sites to the pore space. As a result, gas molecules concentrate inside the pores of the MOF by (selectively) adsorbing onto the pore walls. The amount of gas adsorbed in a MOF at thermodynamic equilibrium depends upon the chemical potential of each component in the gas phase (and the temperature). Therefore, observation of the total mass of gas adsorbed in a MOF [15]—or some other property that depends on the gas adsorbed in the MOF, such as electrical resistance [16, 17], color [18], luminescence [19, 20], or strain [21, 22]—provides information about the composition of the gas. Figure 1 illustrates a miniaturized gravimetric, MOF-based sensor composed of a quartz crystal microbalance (QCM) coated with a thin film of MOF [23, 24]—a surface-mounted MOF [25]. Nanogram-scale changes in the adsorbed mass of gas in the MOF film can be inferred from changes in the resonant frequency of the piezoelectric quartz crystal, forced by an alternating voltage [9, 10]. Several gravimetric, MOF-based sensors have been experimentally demonstrated using QCMs [15, 26-32] and surface acoustic wave devices [33–35] as electromechanical signal transducers [36].

Cross-sensitivity plagues gas sensors in practical applications where the gas contains multiple components that vary in concentration [39]. In the case of MOF-based gas sensors, interfering gas species, in addition to the analyte species, adsorb into the MOF and contribute to the response (i.e. the total adsorbed mass of gas). As a consequence, the inverse problem [40] of inferring the concentration of the analyte from a single-sensor response is underdetermined [41]. To address the problem of cross-sensitivity, one might propose to design a MOF with a very high adsorptive selectivity for the analyte. However, this strategy may be difficult or impossible, and it requires a different MOF highly tailored to each sensing task.

Gas sensor arrays tackle the issue of cross-sensitivity by monitoring the response of a diverse set of (likely, cross-sensitive) MOFs [42, 43], analogous to the mammalian olfactory system (MOFs::olfactory receptors) [44]. Each response of a cross-sensitive MOF, though having contributions from the analyte *and* interferents, places one constraint on the

gas composition. As a whole, the response vector of the gas sensor array may provide sufficient information to uniquely determine the gas composition. Typically, a machine learning algorithm is used to parse the high-dimensional response of a sensor array [45]. A few MOF-based gas sensor arrays have been experimentally demonstrated [16, 29, 46–48]. Still, even gas sensor arrays are susceptible to cross-sensitivity; the inverse problem (determine the gas composition from the sensor array response vector) could still be underdetermined—particularly, if the number of MOFs comprising the array is less than the number of degrees of freedom in the gas composition. In an environment with complex, multicomponent gas mixtures, if the sensor array contains too few MOFs, the information contained in its response is insufficent to fully constrain the gas composition.

In this article, we outline a mathematical method to identify changes in the gas composition to which reversible⁶, quantitative gas sensors/sensor arrays are unresponsive. Gas sensing can be viewed as the inverse problem of finding the gas composition consistent with the sensor response governed by a mixed-gas adsorption model [40]. Owing to cross-sensitivity, the mapping, under the adsorption model, from gas composition space to sensor array response space could be noninjective (many-to-one). Consequently, some gas composition changes are undetectable. By definition, when the gas composition changes in an unresponsive direction in composition space, the sensor response remains constant; the explanation is that the adsorption of one set of species balances (in mass) the desorption of another set of species. These undetectable gas composition changes generally depend upon the initial composition. The identification of unresponsive directions of gas sensors/sensor arrays is important for understanding their limitations and vulnerabilities to adversarial attacks [49].

Specifically, we show that the singular value decomposition (SVD) of the Jacobian matrix of the mapping from gas composition vectors to sensor response vectors is key to determining unresponsive directions and responsive directions, ranked by sensitivity, in composition space. In particular, the unresponsive subspace is the null space of the Jacobian matrix. We illustrate this under the context of quantitative sensing for diluents and higher-hydrocarbons in natural gas [50] (N₂, CO₂, and C₂H₆ in CH₄) using gravimetric, MOF-based sensors comprised of HKUST-1 and Co-MOF-74. We use experimental gas adsorption data and ideal adsorbed solution theory [51, 52] to model the mass of adsorbed gas in each MOF in response to different gas compositions. Under several case studies, we visualize the unresponsive subspace and ranked responsive directions together with the underlying mixed gas adsorption model.

Several computational and mathematical modeling approaches have been developed to design/analyze gas sensor

⁶ Gas sensors based on physical adsorption in stable MOFs lacking adsorption/desorption hysteresis are *reversible*. Suppose the gas composition changes from (i) a reference composition to (ii) some new composition, then (iii) back to the reference composition. The equilibrium mass of gas adsorbed in the MOF will be the same in (i) and (iii).

Table 1. Description of variables/functions.

Symbol	Description			
M	Number of MOFs in the sensor array			
G + 1	Number of species in the gas phase			
X	Mole fraction vector describing gas composition			
m	Sensor array response vector			
\mathcal{X}	Gas composition space, $\mathbf{x} \in \mathcal{X} \subset \mathbb{R}^G$			
\mathcal{M}	Sensor response space, $\mathbf{m} \in \mathcal{M} \subset \mathbb{R}^M$			
\mathbf{x}_{op}	Operating point in gas composition space			
\mathbf{m}_{op}	Sensor response at \mathbf{x}_{op}			
$a(\mathbf{x})$	Adsorption function, maps gas composition to sensor response			
$\tilde{\mathcal{B}} = \tilde{\mathcal{B}}(\mathbf{x}_{op})$	Unresponsive subspace of sensor array			
$\tilde{\mathcal{B}} = \tilde{\mathcal{B}}(\mathbf{x}_{op})$ $\mathbf{J} = \mathbf{J}(\mathbf{x}_{op})$	Jacobian matrix of $a(\mathbf{x})$			
\mathbf{u}_i	Left singular vector i of \mathbf{J}			
\mathbf{v}_i	Right singular vector i of \mathbf{J}			
σ_i	Singular value i of J			

arrays of MOFs [40, 41, 53–57]. Our work focuses on identifying the limitations of non-injective, MOF-based gas sensor arrays by elucidating directions in composition space in which the gas sensor is unresponsive to changes.

2. A mathematical model of gas sensor arrays

2.1. Problem setup

Suppose a gravimetric sensor array of M MOFs aims to determine the composition of a gas (temperature, pressure fixed) with G+1 components. Table 1 summarizes our notation.

The gas composition vector. Let $\mathbf{x} \in \mathbb{R}^G$ be the gas composition vector, with x_i the mole fraction of component i in the gas phase. We omit component G+1 of the gas from \mathbf{x} since its mole fraction follows from $x_{G+1} = 1 - (x_1 + x_2 + \cdots + x_G)$. Thus, the only constraints on \mathbf{x} are $\sum_{i=1}^G x_i \leqslant 1$ and $\mathbf{x} \geqslant \mathbf{0}$. We define this subset of \mathbb{R}^G as gas composition space \mathcal{X} , so that $\mathbf{x} \in \mathcal{X}$. We assume the gas is held at constant pressure and temperature, implying (i) \mathbf{x} fully specifies the thermodynamic state of the gas phase and (ii) G is the number of degrees of freedom in the gas phase.

The sensor response vector. Let $\mathbf{m} \in \mathbb{R}^M$ be the sensor array response vector, with m_i (g gas/g MOF) denoting the *total* mass of gas adsorbed in MOF i at thermodynamic equilibrium, normalized by the mass of MOF in the sensor. We assume, as in practice, that each MOF is cross-sensitive. As a result, m_i is comprised of contributions from each of the G+1 components of the gas phase.

The adsorption function. Mathematically, we view gas sensor arrays as mapping from gas composition space \mathcal{X} to sensor response space $\mathcal{M} \subset \mathbb{R}^M$ [41, 58]. The adsorption function $a: \mathbf{x} \mapsto \mathbf{m}$ maps each gas composition vector $\mathbf{x} \in \mathcal{X}$ to a sensor response vector $\mathbf{m} \in \mathcal{M}$. I.e. $\mathbf{m} = a(\mathbf{x})$ is a model for the total mass of gas adsorbed in each MOF (at thermodynamic equilibrium) as a function of the gas composition. We assume $a(\mathbf{x})$ is a continuously differentiable function, disallowing adsorption/desorption hysteresis, gas-induced first-order structural transitions, and condensation of adsorbates in the pores. We also disallow chemical

transformations in the MOF. The sensor response space $\mathcal{M} = a(\mathcal{X})$ is then the image of gas composition space under the adsorption model.

A model of the adsorption function $a(\mathbf{x})$ could be constructed from adsorption data $\mathcal{D} = \{(\mathbf{x}_i, \mathbf{m}_i)\}_{i=1}^n$, with n the number of experiments exposing the sensor array to a gas mixture to observe its response, through various methods including:

- interpolation of \mathcal{D} .
- A statistical mechanical model of gas adsorption [59] whose parameters are identified using \mathcal{D} .
- A statistical machine learning model trained on \mathcal{D} .
- Ideal adsorption solution theory (IAST) [51] applied to pure-component adsorption models constructed from \mathcal{D} .

The source of \mathcal{D} could be experimental gas adsorption measurements or molecular simulations of gas adsorption [60, 61] in the MOFs.

While we write the adsorption function $a(\mathbf{x})$ as a vectorvalued function, the mass of gas adsorbed in each MOF is independent. In other words, we can independently build the adsorption model for each MOF i in the array, $m_i = a_i(\mathbf{x})$.

Gas sensing as an inverse problem [40]. The *forward* problem is to predict the response of the sensor array \mathbf{m} given the gas composition \mathbf{x} . The solution is to evaluate the adsorption model $\mathbf{m} = a(\mathbf{x})$. The *inverse problem* arises in gas sensing: we wish to predict the gas composition \mathbf{x} given the sensor response \mathbf{m} using the adsorption model $\mathbf{m} = a(\mathbf{x})$. While the forward problem always has a unique solution, the inverse problem may have a unique solution, no solution, or many solutions.

2.2. Non-injective gas sensor arrays with underdetermined inverse problems

In this work, we consider gas sensor arrays comprised of fewer MOFs than degrees of freedom in the gas composition (M < G). The mapping $a: \mathbf{x} \mapsto \mathbf{m}$ under a sensor array with M < G is generally non-injective (many-to-one). Consequently, the inverse problem of determining the gas composition \mathbf{x} from the sensor response \mathbf{m} is underdetermined;

typically, many gas compositions can produce the observed response. In the inverse problem, observation of each MOF's response, generally, provides one independent constraint, $m_i = a_i(\mathbf{x})$, on the gas composition. For M < G, the response of the sensor array places an insufficient number of constraints on the gas composition to uniquely determine it.

As a result of their (view 1) non-injective mapping $a: \mathbf{x} \mapsto \mathbf{m}$ and (view 2) underdetermined inverse problems, gas sensor arrays with fewer MOFs than degrees of freedom in the gas (M < G) suffer from unresponsiveness to some changes in gas composition: despite a change in composition, the sensor response remains constant, and hence the composition change goes undetected.

3. Unresponsive and ranked responsive directions of non-injective gas sensors

Non-injective gas sensors contain fewer MOFs than degrees of freedom in the gas composition. They are vulnerable to blindness: the sensor is unresponsive to certain gas composition changes. Our work focuses on identifying these vulnerabilities in non-injective gas sensors. Moreover, the sensor is more sensitive to certain gas composition changes than others (of the same magnitude). We show that the SVD of the Jacobian matrix of the adsorption function $a(\mathbf{x})$ is key to identifying directions in composition space to which the sensor is most, least-, and un-responsive.

3.1. The operating point \mathbf{x}_{op} as a reference

We will define unresponsive and ranked responsive directions in reference to some steady-state, reference gas composition, or *operating point* $\mathbf{x}_{op} \in \mathcal{X}$. $\mathbf{m}_{op} := a(\mathbf{x}_{op})$ is the sensor response at this operating point.

3.2. The unresponsive locus $\mathcal B$

The unresponsive locus $\mathcal{B} \subset \mathcal{X}$ associated with an operating point \mathbf{x}_{op} is the set of gas compositions such that the sensor response remains constant at \mathbf{m}_{op} :

$$\mathcal{B} := \{ \mathbf{x} \in \mathcal{X} : a(\mathbf{x}) = \mathbf{m}_{op} \}. \tag{1}$$

The unresponsive locus is an intersection of the level sets of the adsorption functions for each MOF in the sensor array, $\mathcal{B} = \bigcap_{i=1}^{M} \{\mathbf{x} : a_i(\mathbf{x}) = m_{i,\text{op}}\}$. By definition, the sensor array cannot distinguish between gas compositions in the unresponsive locus. A change in the gas composition from $\mathbf{x}_{\text{op}} \in \mathcal{B}$ to $\mathbf{x}' \in \mathcal{B}$ is undetectable despite $\mathbf{x}' \neq \mathbf{x}_{\text{op}}$. Fundamentally, the response of a sensor array composed of cross-sensitive MOFs remains constant under the composition change from \mathbf{x}_{op} to \mathbf{x}' because the adsorption of one set of species balances (in mass) the desorption of another set of species (see figure 2). A physically trivial example of a mathematically non-trivial unresponsive locus is when all MOFs do not adsorb a particular component of the gas.

3.3. Linear approximation of $a(\mathbf{x})$ near the operating point \mathbf{x}_{op}

Let us make a linear approximation $\tilde{a}(\mathbf{x})$ of the adsorption function $a(\mathbf{x})$ valid near the operating point \mathbf{x}_{op} . A first-order

Taylor expansion of $a(\mathbf{x})$ about \mathbf{x}_{op} gives:

$$a(\mathbf{x}) \approx a(\mathbf{x}_{\text{op}}) + \mathbf{J}(\mathbf{x}_{\text{op}})(\mathbf{x} - \mathbf{x}_{\text{op}}) =: \tilde{a}(\mathbf{x}),$$
 (2)

with $\mathbf{J} = \mathbf{J}(\mathbf{x})$ the $M \times G$ Jacobian matrix of $a(\mathbf{x})$ with $J_{ij} := \frac{\partial m_i}{\partial x_j}$. For a non-injective gas sensor array (M < G), \mathbf{J} is fat. From a geometric viewpoint, the approximator $m_i \approx \tilde{a}_i(\mathbf{x})$ is a hyperplane tangent to the surface $a_i(\mathbf{x})$ and passing through $m_{i,\text{op}}$.

3.4. The (local) unresponsive subspace of composition space

We define the (locally valid) unresponsive subspace $\tilde{\mathcal{B}} \subset \mathbb{R}^G$ of a sensor array associated with operating point \mathbf{x}_{op} as the directions in composition space such that, for small changes in the gas composition in these directions, the sensor response remains approximately constant at \mathbf{m}_{op} . Thus, for a unit vector $\Delta \mathbf{x} \in \tilde{\mathcal{B}}$, $a(\mathbf{x}_{op} + \epsilon \Delta \mathbf{x}) \approx a(\mathbf{x}_{op})$ with ϵ a small number. Invoking the linear approximation in equation (2), the local unresponsive subspace is given by the null space of the Jacobian matrix $\mathbf{J}(\mathbf{x}_{op})$:

$$\tilde{\mathcal{B}} := \{ \Delta \mathbf{x} \in \mathbb{R}^G : \mathbf{J}(\mathbf{x}_{op}) \Delta \mathbf{x} = \mathbf{0} \}$$
(3)

$$\Rightarrow \tilde{a}(\mathbf{x}_{op} + \Delta \mathbf{x}) = \tilde{a}(\mathbf{x}_{op}) = \mathbf{m}_{op} \quad \forall \ \Delta \mathbf{x} \in \tilde{\mathcal{B}}.$$
 (4)

The null space of **J** will be non-trivial provided G > M. I.e, sensor arrays such that M < G possess non-trivial unresponsive subspaces because the mapping $\tilde{a} : \mathbf{x} \mapsto \mathbf{m}$ is non-injective.

3.5. The sensitive direction in composition space

The sensor response is most sensitive to gas composition changes in the direction of:

$$\Delta \mathbf{x}_{s} := \arg \max_{\Delta \mathbf{x}: \|\Delta \mathbf{x}\| = \epsilon} \|\tilde{a}(\mathbf{x}_{op} + \Delta \mathbf{x}) - \tilde{a}(\mathbf{x}_{op})\|.$$
 (5)

Of all gas composition changes $\Delta \mathbf{x}$ from \mathbf{x}_{op} that are small $(\epsilon>0)$ in magnitude, those in the sensitive direction of $\Delta \mathbf{x}_{s}$ elicit the largest-magnitude change in the response of the sensor array.

3.5.1. The singular value decomposition (SVD) of **J**. The SVD [62, 63] of the $M \times G$ Jacobian matrix **J** factorizes it as:

$$\mathbf{J} = \mathbf{U} \mathbf{\Sigma} \mathbf{V}^{\mathsf{T}},\tag{6}$$

where **U** is an $M \times M$ orthogonal matrix, Σ is an $M \times G$ diagonal matrix with singular values $\sigma_1 \geqslant \sigma_2 \geqslant \ldots \geqslant \sigma_M$ listed down the diagonal, and **V** is a $G \times G$ orthogonal matrix. The left singular vector $\mathbf{u}_i \in \mathbb{R}^M$ is column i of **U** and lies in sensor response space. The right singular vector $\mathbf{v}_i \in \mathbb{R}^G$ is column i of **V** and lies in gas composition space⁷. The M left (G right) singular vectors form an orthonormal basis for sensor response (gas composition) space. Provided the MOFs are distinct, it is

⁷ Technically, the singular vectors can/will lie outside the *valid* sensor response/gas composition spaces as we've defined them since e.g. they can have negative entries.

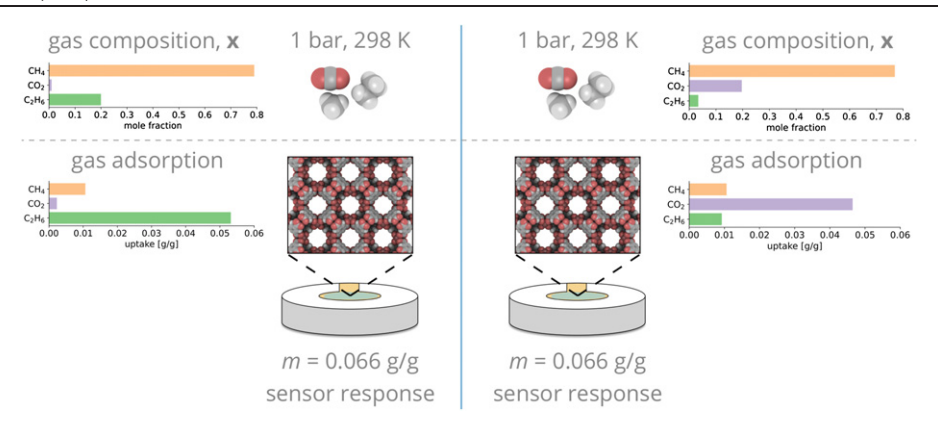


Figure 2. Illustrating a gas composition change to which a non-injective, gravimetric, MOF-based gas sensor is unresponsive. A single QCM-HKUST-1 sensor is immersed in a gas mixture of two different compositions: on the left, a dominantly CH_4/C_2H_6 mixture; on the right, a dominantly CH_4/C_0 mixture. The response of the sensor to the two distinct gas compositions is identical; hence, the sensor cannot be used to distinguish between these two compositions. The total mass of gas adsorbed in the HKUST-1 film remains the same upon changing from the $\sim CH_4/C_0H_6$ to $\sim CH_4/C_0H_6$ mixture because the desorption of C_2H_6 approximately balances (in mass) the adsorption of CO_2 , while the adsorption of CH_4 remains approximately constant.

extremely likely that **J** is full-rank (rank M)⁸, so we assume $\sigma_M > 0$.

Seen by $JV = U\Sigma$:

$$\mathbf{J}\mathbf{v}_{i} = \begin{cases} \sigma_{i}\mathbf{u}_{i} & i \in \{1, 2, \dots, M\} \\ \mathbf{0} & i \in \{M+1, M+2, \dots, G\}. \end{cases}$$
(7)

Therefore, under the linear approximation $\tilde{a}(\mathbf{x})$ in equation (2), the sensor array is:

- responsive to gas composition changes in directions belonging to the subspace spanned by the first M right singular vectors ($\mathbf{v}_1, \mathbf{v}_2, \dots, \mathbf{v}_M$). This list of vectors is ranked by the magnitude of the associated sensor array responses.
- Unresponsive to gas composition changes in directions belonging to the subspace spanned by the set of last G M right singular vectors $\{\mathbf{v}_{M+1}, \mathbf{v}_{M+2}, \dots, \mathbf{v}_G\}$. This subspace is the null space of \mathbf{J} .

Hence,

- the sensitive direction of the gas sensor array, $\Delta \mathbf{x}_s$ in equation (5), is described by the first right singular vector \mathbf{v}_1 of the Jacobian matrix \mathbf{J} . The gas sensor array is responsive, but less sensitive, to composition changes in the subspace spanned by $\{\mathbf{v}_2, \mathbf{v}_3, \dots, \mathbf{v}_M\}$.
- The local unresponsive subspace $\tilde{\mathcal{B}}$ is spanned by the last (unranked) G M right singular vectors $\{\mathbf{v}_{M+1}, \mathbf{v}_{M+2}, \dots, \mathbf{v}_G\}$ of \mathbf{J} .

We emphasize that the sensitive and unresponsive directions (i) depend on the operating gas composition \mathbf{x}_{op} and (ii) pertain to *small* changes in the gas composition since they rely on the linear approximation in equation (2) of the generally nonlinear function $a(\mathbf{x})$.

We remark on the uniqueness of the SVD in equation (6). The singular values are unique. The left and right singular vectors associated with the distinct, non-zero singular values

are unique, up to both corresponding vectors being multiplied by -1. The right singular vectors spanning the null space are much more arbitrary in the sense that they can be any orthonormal basis for the null space.

Note, if the response vector is recorded in units g gas instead of g gas/g MOF, (i) the responsive and unresponsive *subspaces* do not change, but (ii) the ranked responsive directions that span the responsive subspace do change if different masses of MOF are used in each sensor.

3.6. Special case: linear adsorption model

Suppose gas adsorption in each MOF of the array is described by Henry's law:

$$m_i = \sum_{i=1}^{G+1} H_{i,j} P x_j, \tag{8}$$

with P the total pressure (bar) of the gas phase and $H_{i,j}$ the Henry coefficient (g gas/(g MOF-bar)) of gas j in MOF i. Imposing the constraint that the mole fractions $\{x_j\}$ sum to one, the adsorption model for the sensor array is linear:

$$\mathbf{m} = a(\mathbf{x}) = \mathbf{A}\mathbf{x} + \mathbf{b},\tag{9}$$

with $A_{ij} := P(H_{i,j} - H_{i,G+1})$, $b_i := PH_{i,G+1}$, and $\mathbf{x} := [x_1, x_2, \dots, x_G]$. Under this special case, the Jacobian matrix $\mathbf{J} = \mathbf{A}$ does not depend on a reference gas composition \mathbf{x}_{op} . Therefore, the unresponsive and responsive subspaces are independent of \mathbf{x}_{op} , too.

4. Summarizing with a toy example

We illustrate the identification of the unresponsive and ranked responsive directions with a toy example: a sensor array of M = 2 distinct MOFs aimed at sensing a quaternary mixture at fixed temperature and pressure (G = 3). See figure 3(a).

Figure 3(c) illustrates the SVD of an $M = 2 \times 3 = G$ Jacobian matrix $\mathbf{J} = \mathbf{J}(\mathbf{x}_{op})$ at some operating point \mathbf{x}_{op} . The three orthonormal right singular vectors $\{\mathbf{v}_1, \mathbf{v}_2, \mathbf{v}_3\}$ lie in $G = \mathbf{v}_1$

⁸ J could, however, be ill-conditioned [40].

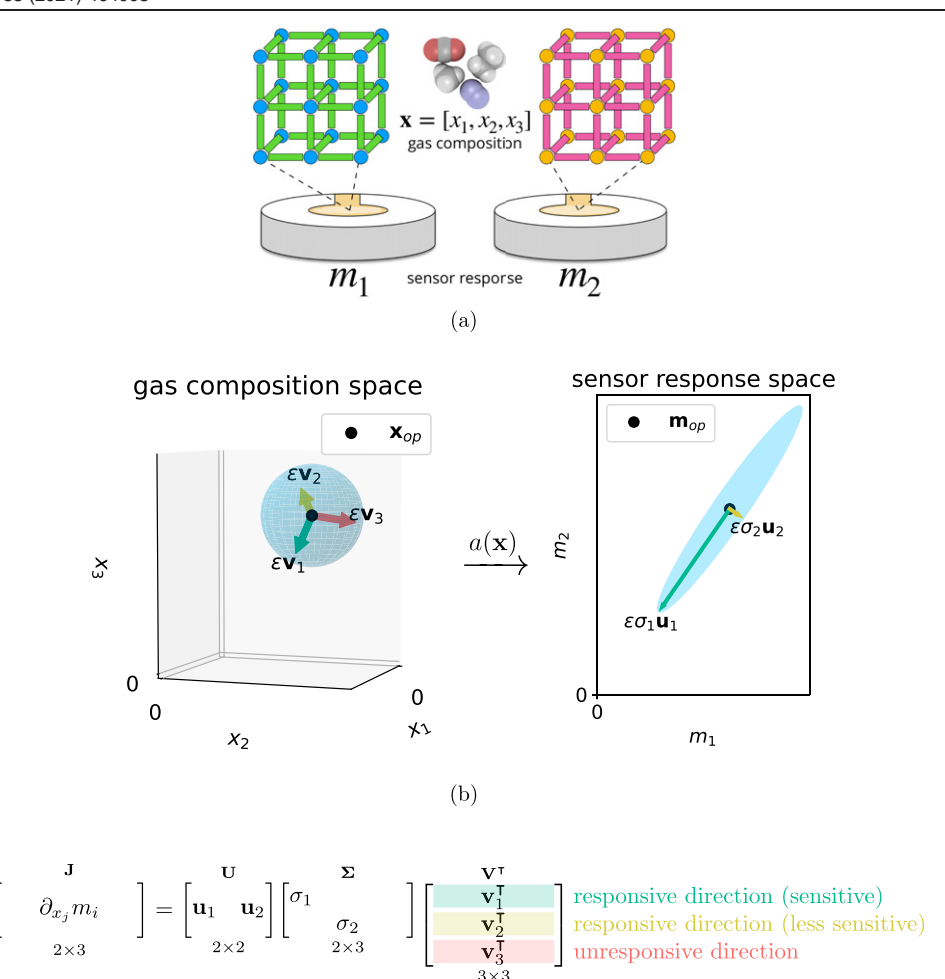


Figure 3. Elucidating the unresponsive and ranked responsive directions of a (toy) sensor array through the SVD of the Jacobian matrix $\bf J$ of its adsorption function $a({\bf x})$. (a) A gravimetric, two-MOF sensor array immersed in a four-component gas mixture at constant temperature and pressure but varying composition. The gas composition ${\bf x} \in \mathbb{R}^3$, while the sensor response ${\bf m} \in \mathbb{R}^2$. (b) The adsorption function $a({\bf x})$ is a map $a: {\bf x} \mapsto {\bf m}$ from 3D gas composition space (left) to 2D sensor response space (right). The operating gas composition ${\bf x}_{\rm op}$ and associated response ${\bf m}_{\rm op}$ are shown as black points. Under the linear approximation of $a({\bf x})$ valid locally around ${\bf x}_{\rm op}$: the image of the sphere of small radius ϵ (blue, left) maps to the solid ellipse (blue, right) with semi-major and semi-minor axes given by $\epsilon \sigma_1 {\bf u}_1$ and $\epsilon \sigma_2 {\bf u}_2$, respectively. Gas composition changes $\epsilon {\bf v}_1, \epsilon {\bf v}_2, \epsilon {\bf v}_3$ form an orthogonal basis of composition space and are mapped to response changes $\epsilon \sigma_1 {\bf u}_1, \epsilon \sigma_2 {\bf u}_2, {\bf 0}$, respectively. ${\bf v}_3$ describes the unresponsive direction, since small changes in composition in this direction do not alter the response. Small composition changes in the direction of ${\bf v}_1$ elicit the largest-magnitude response. (c) The SVD ${\bf J} = {\bf U} {\bf \Sigma} {\bf V}^{\rm T}$ gives the vectors described in (b).

(c)

3-dimensional composition space, while the two orthonormal left singular vectors $\{\mathbf{u}_1, \mathbf{u}_2\}$ lie in M = 2-dimensional response space. The Jacobian matrix maps the right-singular vectors into response space as follows:

$$\mathbf{J}\mathbf{v}_1 = \sigma_1 \mathbf{u}_1 \tag{10}$$

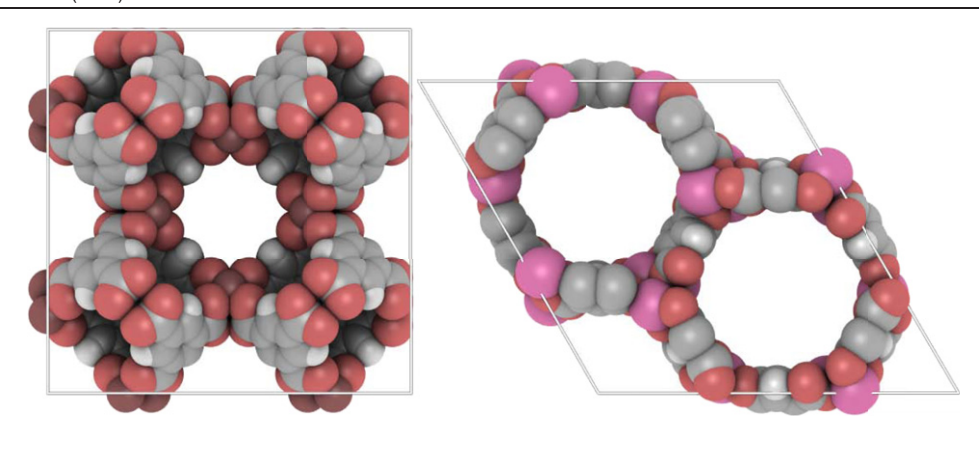
$$\mathbf{J}\mathbf{v}_2 = \sigma_2 \mathbf{u}_2 \tag{11}$$

$$\mathbf{J}\mathbf{v}_3 = \mathbf{0}.\tag{12}$$

Provided the MOFs are distinct, the two rows of **J** are highly unlikely to point in exactly the same direction; thus, we safely assume **J** is full-rank, i.e. $\sigma_2 > 0$. Equations (10) and (11) indicate the sensor is responsive to gas composition changes in the direction of \mathbf{v}_1 and \mathbf{v}_2 but more sensitive to changes in the direction of \mathbf{v}_1 ($\sigma_1 \geqslant \sigma_2$ by definition, but likely $\sigma_1 > \sigma_2$). Equation (12) indicates the null space of the

Jacobian matrix is non-trivial and spanned by \mathbf{v}_3 . Therefore, the linear map $\tilde{a}: \mathbf{x} \mapsto \mathbf{m}$ is non-injective, as a consequence of M < G.

Consider small gas composition changes (of magnitude $\epsilon > 0$) from \mathbf{x}_{op} . The linear approximant $\tilde{a}(\mathbf{x})$ in equation (2) maps a sphere in 3D composition space centered at \mathbf{x}_{op} to a solid ellipse in 2D sensor response space [62] centered at \mathbf{m}_{op} . See figure 3(b). This follows from equation (2) and equations (10)–(12). The composition change in the sensitive direction, $\epsilon \mathbf{v}_1$ (green in figure 3(b)), elicits the largest sensor response—from \mathbf{m}_{op} to $\mathbf{m}_{op} + \epsilon \sigma_1 \mathbf{u}_1$ on the endpoint of the major axis of the ellipse. The sensor is responsive, but less sensitive, to composition changes in the direction of \mathbf{v}_2 (yellow in figure 3(b)); the composition change $\epsilon \mathbf{v}_2$ moves the sensor response by the vector $\epsilon \sigma_2 \mathbf{u}_2$, placing it on the endpoint of the minor axis of the ellipse. The relative sensitivity of the



HKUST-1 Co-MOF-74 CH₄ CH₄ N_2 N_2 CO_2 CO₂gas uptake [g gas/g MOF] gas uptake [g gas/g MOF] C₂H₆ C₂H₆ 10 Langmuir model 10 Quadratic model Langmuir model Langmuir model Langmuir model DSLangmuir model Langmuir model Quadratic model 10^{-2} 10^1 10^{-1} 10² 10 10-100 10-100 104 pressure [bar] pressure [bar]

(a)

Figure 4. The two MOFs as candidate recognition elements and their equilibrium, pure-component gas adsorption isotherms. (a) The crystal structures of HKUST-1 [37] (left) and Co-MOF-74 [64] (right). (b) Experimentally measured, pure-component CH_4 (298 K) [67, 71], N_2 (298 K) [70, 71], CO_2 (298 K) [68, 71], and C_2H_6 (296 K) [69] adsorption isotherm data (points) in HKUST-1 and Co-MOF-74. Curves show the pure-component adsorption models fit to the data.

(b)

response to composition changes in the direction of \mathbf{v}_1 vs \mathbf{v}_2 depends on the singular values, σ_1 vs σ_2 . On the other hand, \mathbf{v}_3 is the unresponsive direction; the composition change $\epsilon \mathbf{v}_3$ (red in figure 3(b)) does not elicit a sensor response, and \mathbf{m} remains at \mathbf{m}_{op} despite the change in gas composition. Using this toy sensor array, we therefore cannot detect small composition changes in the direction of \mathbf{v}_3 !

5. Demonstration: natural gas sensing with gravimetric sensors based on HKUST-1 and Co-MOF-74

We now demonstrate the identification of the unresponsive subspace and ranked responsive directions in gas composition space for a gravimetric, single-MOF sensor and two-MOF sensor array for diluents and higher-hydrocarbons in natural gas [50]. Specifically, suppose the sensor (array) is immersed in a variable-composition gas mixture involving N_2 , C_2H_6 , CO_2 , and CH_4 at 1 bar and 298 K. We consider two candidate MOFs as the recongition element(s), HKUST-1 [37] and Co-MOF-74 [64]. HKUST-1 is composed of dicopper(II) ions coordinated to benzene-1,3,5-tricarboxylate ligands to form three distinct pores, two of \sim 1.4 nm and one of \sim 1.0 nm in diameter [65]. Co-MOF-74 is composed of cobalt(II) ions coordinated to 2,5-dihydroxyterephthalic acid ligands to form hexagonal channels of \sim 1.2 nm diameter [66]. Figure 4(a) visualizes their crystal structures.

In each case study below, the number of degrees of freedom in the gas composition is greater than the number of MOFs comprising the sensor/sensor array (G > M). Thus, (i) the sensor's mapping under a from gas composition space to sensor response space is non-injective and (ii) the inverse problem to determine the gas composition from the sensor response is underdetermined. Accordingly, the sensor (array) will contain a non-trivial unresponsive subspace.

Table 2. References for experimentally measured, pure-component, equilibrium gas adsorption isotherms at 298 K (except C_2H_6 , at 296 K).

MOF	$\mathrm{CH_4}$	CO_2	C_2H_6	N_2
HKUST-1	[67]	[68]	[69]	[70]
Co-MOF-74	[71]	[71]	[69]	[71]

5.1. The adsorption model $a(\mathbf{x})$, its Jacobian matrix \mathbf{J} , and its SVD

We construct an adsorption model for each MOF on the basis of experimentally measured, pure-component CH_4 , CO_2 , C_2H_6 , and N_2 adsorption data at or near 298 K. Figure 4(b) displays the adsorption isotherms and table 2 provides the references.

We invoke ideal adsorbed solution theory (IAST) [51, 52] and use pyIAST [72] to implement the adsorption function $a(\mathbf{x})$. Section 2.1 explains that $a(\mathbf{x})$ gives the total mass of gas adsorbed in each MOF (g/g) of the array as a function of the gas composition \mathbf{x} . IAST is a thermodynamic framework to predict mixed-gas adsorption from pure-component adsorption isotherms. Figure 4(b) shows the pure-component adsorption isotherm models fit to the experimental adsorption data and used as input for IAST calculations; the single-site Langmuir, dual-site (DS) Langmuir, and quadratic adsorption isotherm models fit the data well. N.b., though we write $\mathbf{m} = a(\mathbf{x})$, IAST provides $m_i = a_i(\mathbf{x})$ for each MOF in the array independently.

We compute the Jacobian matrix $J = J(x_{op})$ of a(x) numerically via a second-order, centered finite difference using numdifftools; we compute the SVD of J using numpy.

5.2. Case M = 1, G = 2: single-MOF sensor, ternary gas mixture

We first consider a single-MOF sensor, using either Co-MOF-74 or HKUST-1, immersed in a three-component mixture: CH₄/N₂/CO₂, CH₄/N₂/C₂H₆, or CH₄/C₂H₆/CO₂ at 1 bar and 298 K.

Figure 5 visualizes, under these six scenarios, the adsorption function $m = a(\mathbf{x})$ as well as the unresponsive $\mathbf{v_2}$ (red arrow) and sensitive v_1 (green arrow) directions—given by the right singular vectors of the Jacobian matrix $\mathbf{J}(\mathbf{x}_{op})$ — at a reference gas composition \mathbf{x}_{op} (black dot). The rows correspond to the three different gas mixtures; the columns correspond to the two different single-MOF sensors. Each panel displays the 2D gas composition space pertaining to the row. The colored lines are contours of the adsorption function $a(\mathbf{x})$ and are labeled by the total adsorbed mass of gas m in the respective single-MOF sensor. Each map $a: \mathbf{x} \mapsto m$ is clearly noninjective, as an unresponsive locus of points elicits the same sensor response m. Within each panel, (i) the nonlinearity of the contours and the different areas between successive contours reflect the nonlinearity of $a(\mathbf{x})$ and (ii) the slant of the contours reflects the different affinity for the MOF among the three different components of the gas.

The sensitive direction \mathbf{v}_1 is orthogonal to the contour $\{\mathbf{x}:$ $a(\mathbf{x}) = m_{\text{op}}$. Among all fixed-magnitude changes in gas composition, the change in the sensitive direction will elicit the largest response (see equation (5)). The unresponsive direction is tangential to the contour $\{\mathbf{x} : a(\mathbf{x}) = m_{\text{op}}\}$. The unresponsive subspace is one-dimensional owing to the single constraint imposed by the response of the sensor on the two degrees of freedom in the gas composition. For a small change in gas composition in the unresponsive direction, the sensor response remains approximately the same and, hence, the composition change is not detected by the sensor. Figure 2 illustrates the underlying physical cause of the unresponsiveness to a composition change, using as an example the HKUST-1 sensor immersed in a CH₄/C₂H₆/CO₂ mixture: the desorption of one set of species balances (in mass) the adsorption of another set of species.

For the two gas mixtures involving N_2 , the sensitive direction is oriented approximately in the direction of changes in the more readily adsorbing components, CO_2 or C_2H_6 . N_2 -MOF interactions are weaker than CO_2 - and C_2H_6 -MOF interactions, reflected in the adsorption isotherms in figure 4(b). The $CH_4/C_2H_6/CO_2$ mixture is most interesting, as the sensitive and unresponsive directions each have significant components in the direction of changes in CO_2 and C_2H_6 mole fractions. Again reflected in the adsorption isotherms in figure 4(b), CO_2 -MOF and C_2H_6 -MOF interactions are competitive.

Comparing Co-MOF-74 and HKUST-1 for CH₄/C₂H₆/CO₂ sensing, the sensitive direction \mathbf{v}_1 for HKUST-1 has a larger component along $\mathbf{x} = [0.5, 0.5]$ (see figure 5). Therefore, HKUST-1 is a more suitable sensor for estimating the *sum* of the CO₂ and C₂H₆ mole fractions and, thus, the mole fraction of CH₄. In other words, the component of the unresponsive direction for HKUST-1 along $\mathbf{x} = [0.5, 0.5]$ is smaller than for Co-MOF-74; so, HKUST-1 is not as blind as Co-MOF-74 to changes in the CH₄ mole fraction in the CH₄/C₂H₆/CO₂ mixture. Figure 6 clarifies: observation of the response m_{op} of the HKUST-1 sensor places tighter bounds on x_{CH_4} than observation of the response of the Co-MOF-74 sensor because $x_{\rm CH_4}$ is approximately constant along its unresponsive direction. This exemplifies how unresponsive directions and loci could be used to juxtapose two non-injective sensors. However, a more rigorous comparison of the two sensors should include sensitivity to measurement noise [40, 55].

5.3. Case M = 1, G = 3: single-MOF sensor, quaternary gas mixture

Now consider a single-MOF sensor—either Co-MOF-74 or HKUST-1— immersed in a CH₄/N₂/CO₂/CH₄ mixture at 1 bar and 298 K.

Figure 7 visualizes the adsorption function $m = a(\mathbf{x})$ by showing its level sets in 3D gas composition space, colored by the associated response m. The black point is the reference gas composition $\mathbf{x}_{\rm op}$. The sensitive direction \mathbf{v}_1 (green vector) is orthogonal to the level set $\{\mathbf{x}: a(\mathbf{x}) = m_{\rm op}\}$, and the unresponsive subspace, a plane spanned by \mathbf{v}_2 and \mathbf{v}_3 (red vectors), is tangent to it. Note the vectors \mathbf{v}_2 and \mathbf{v}_3

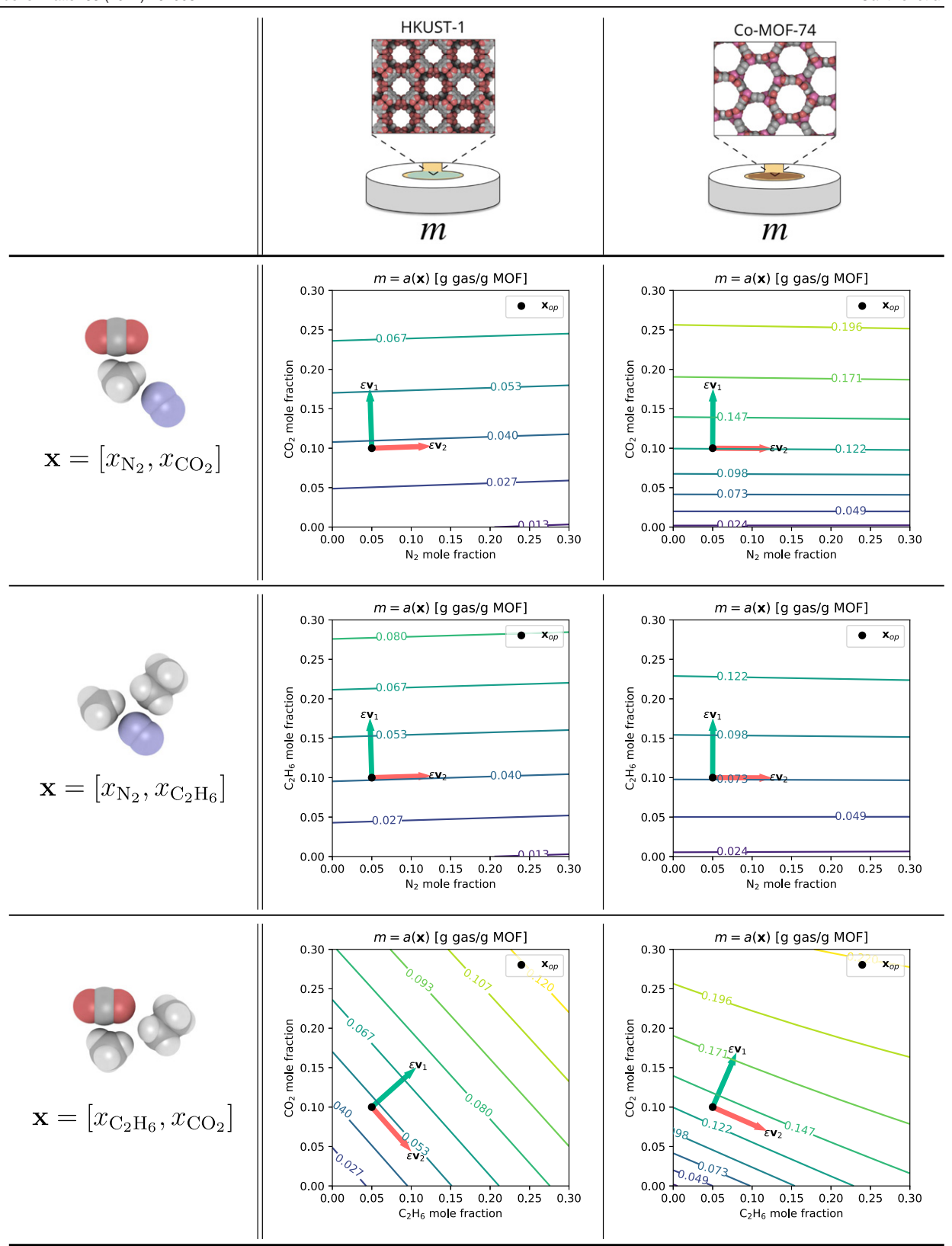


Figure 5. Case M=1, G=2: visualization of $a(\mathbf{x})$ and the unresponsive and sensitive directions for a single-MOF sensor immersed in a three-component gas mixture at 1 bar and 298 K under six distinct cases. The row indicates which three species compose the gas mixtures. The column indicates which MOF is used as the recognition element for the gravimetric sensor. In each panel, the plane represents gas composition space. Color-coded contours of the adsorption function $a(\mathbf{x})$ are drawn to indicate unresponsive loci and are labeled with $m=a(\mathbf{x})$ for all \mathbf{x} on that contour. At the operating gas composition \mathbf{x}_{op} , the sensitive (green) and unresponsive (red) directions are shown as $\epsilon \mathbf{v}_1$ and $\epsilon \mathbf{v}_2$, respectively ($\epsilon=1/15$).

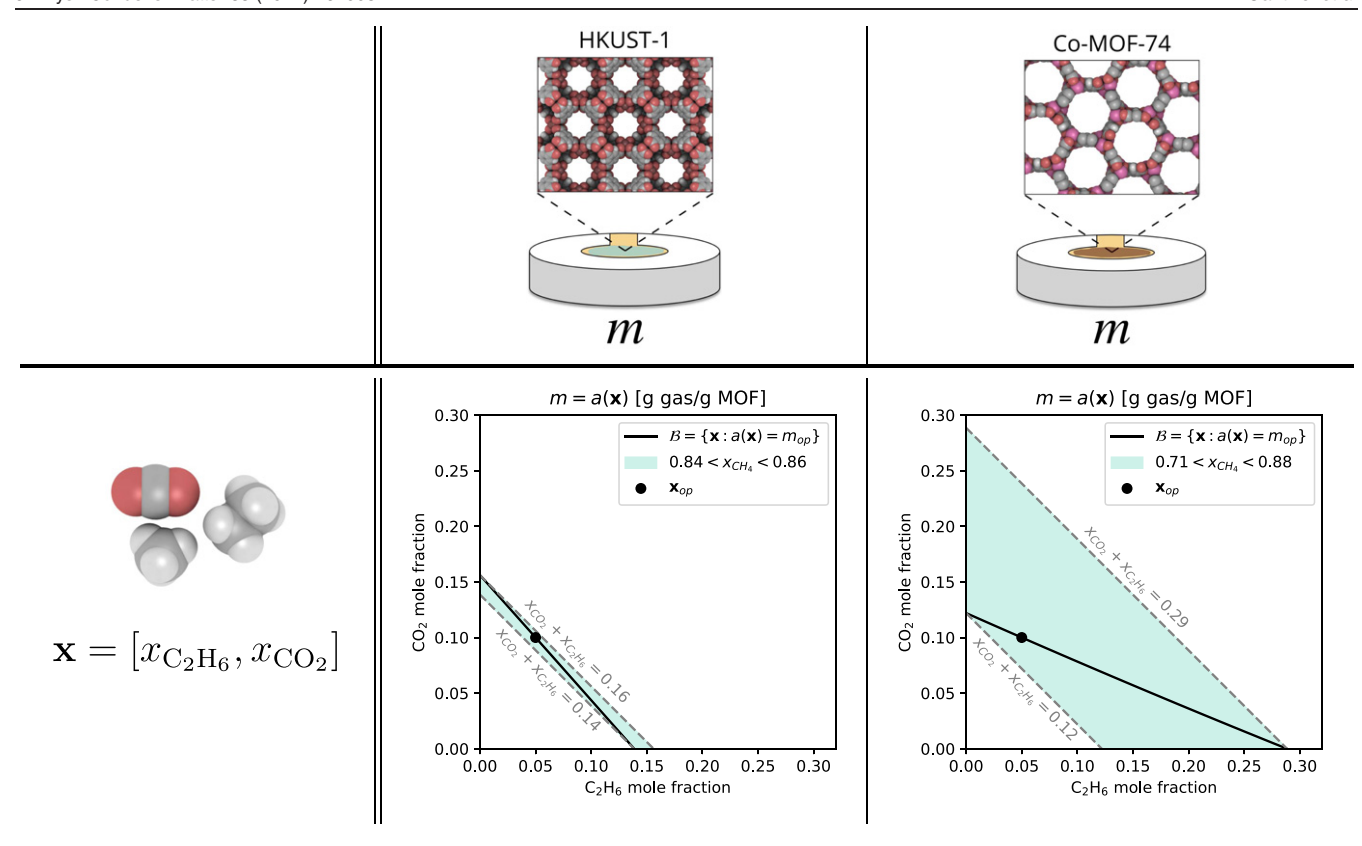


Figure 6. Case M=1, G=2: comparing the utility of two non-injective gas sensors for determining x_{CH_4} in a CH₄/C₂H₆/CO₂ mixture. Along the unresponsive locus \mathcal{B} (black curve) associated with \mathbf{x}_{op} (black dot), the response of the sensor remains fixed at m_{op} . Observation of the response m_{op} in each sensor places a lower and upper bound on the mole fraction of CH₄, x_{CH_4} . The HKUST-1 sensor gives a more useful constraint on x_{CH_4} than the Co-MOF-74 sensor; x_{CH_4} is constrained to lie in a smaller interval by the response of the HKUST-1 sensor.

are not ranked, i.e. one is not more or less unresponsive than the other, and are not unique, in that any two orthonormal vectors that lie in the unresponsive plane can be chosen. The unresponsive subspace is two-dimensional due to the single constraint imposed by the response of the sensor on the three degrees of freedom in the gas composition. Small changes in gas composition on the unresponsive plane are undetectable since the sensor response remains constant. The sensitive direction \mathbf{v}_1 is orthogonal to the unresponsive plane.

Comparing the sensitive directions of the two sensors at the operating point

$$\mathbf{x}_{\text{op}} = [0.25, 0.2, 0.2] \tag{13}$$

we find, for HKUST-1 and Co-MOF-74, respectively:

$$\mathbf{v_1} \approx \begin{bmatrix} -0.02 & 0.67 & 0.74 \end{bmatrix}$$
 (14)

$$\mathbf{v_1} \approx \begin{bmatrix} 0.02 & 0.96 & 0.27 \end{bmatrix}$$
 (15)

with the gas composition vector defined as:

$$\mathbf{x} = [x_{\text{N}_2}, x_{\text{CO}_2}, x_{\text{C}_2 \text{H}_6}]. \tag{16}$$

Both sensors are much more sensitive to changes in CO_2 and C_2H_6 than to changes in N_2 . Note the three faces of each cube in figure 7 when one mole fraction is set to zero are equivalent to figure 5.

5.4. Case M = 2, G = 3: two-MOF sensor array, quaternary gas mixture

Now consider a two-MOF sensor array, comprised of Co-MOF-74 and HKUST-1, immersed in a $CH_4/N_2/CO_2/CH_4$ mixture. See figure 8(a).

Figure 8(b) is a visualization to understand the mapping $a: \mathbf{x} \mapsto \mathbf{m}$, with \mathbf{x} in a 3D gas composition space and \mathbf{m} in a 2D sensor response space. The image of the sphere of radius $\epsilon = 0.04$ in gas composition space (blue, left) is the solid ellipse-like shape (blue, right) in sensor response space; they are (approximately, for the case of the ellipse-like shape) centered, respectively, at the reference gas composition \mathbf{x}_{op} and its associated response \mathbf{m}_{op} . Unlike the M=2, G=3 case in the toy sensor array figure 3(b), the image of the sphere is not exactly a solid ellipse owing to the nonlinearity of $a(\mathbf{x})$.

Magnitude- ϵ changes in the gas composition in the sensitive and intermediate directions in gas composition space—changes of $\epsilon \mathbf{v}_1$ and $\epsilon \mathbf{v}_2$, the green and yellow vectors in figure 8(b)—are mapped to the endpoints of the semimajor-like and semiminor-like axes of the ellipse-like shape— $\epsilon \sigma_1 \mathbf{u}_1$ and $\epsilon \sigma_2 \mathbf{u}_2$, respectively. Among all magnitude- ϵ changes in the gas composition on the sphere (left), a change $\sim \epsilon \mathbf{v}_1$ produces the largest-magnitude sensor array response. The sensor array is responsive to, but with reduced sensitivity, small changes in the intermediate direction \mathbf{v}_2 . On the other hand, the sensor

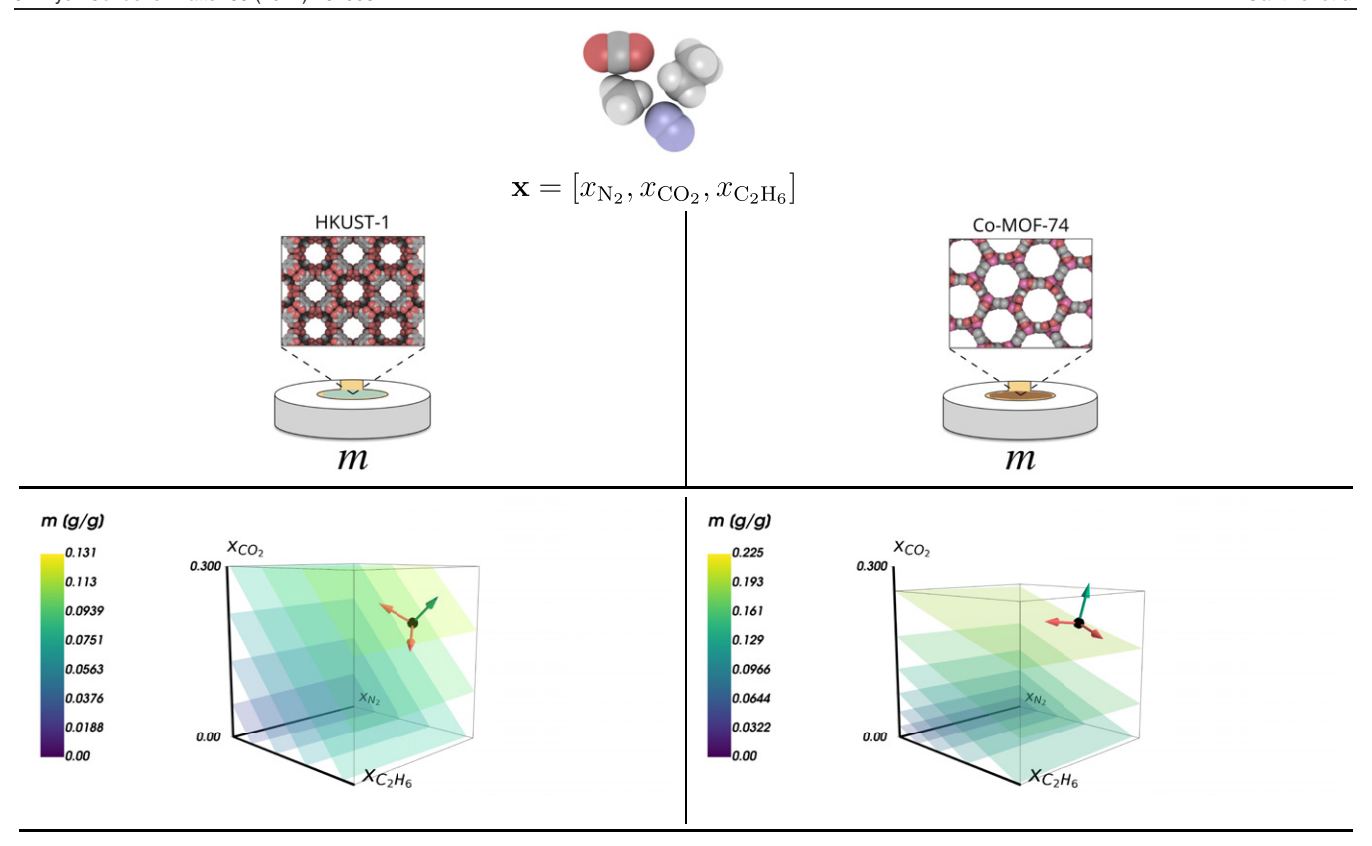


Figure 7. Case M=1, G=3: visualization of $m=a(\mathbf{x})$ and the unresponsive plane and sensitive direction for a single-MOF sensor immersed in a $\mathrm{CH_4/N_2/CO_2/C_2H_6}$ gas mixture at 1 bar and 298 K. The column indicates which MOF is used as the recognition element for the gravimetric sensor. Each panel shows gas composition space. Level surfaces of the adsorption function $a(\mathbf{x})$ are color-coded according to the associated m. At the operating gas composition \mathbf{x}_{op} (black point), (i) the sensitive direction $\epsilon \mathbf{v}_1$ is shown by the green vector and (ii) the unresponsive plane is spanned by the two unresponsive directions $\epsilon \mathbf{v}_2$, $\epsilon \mathbf{v}_3$ shown by the red vectors.

array is unresponsive to small changes in the gas composition in the unresponsive direction of \mathbf{v}_3 . The unresponsive subspace is one dimensional here because the response of the two MOFs places two constraints on the three degrees of freedom in the gas composition.

6. Non-injective gas sensor arrays are not useless

The inverse problem [40] of predicting the gas composition \mathbf{x} from the response vector \mathbf{m} of a non-injective gas sensor array typically has infinite solutions, meaning that infinitely many gas compositions are consistent with the response. We therefore cannot make a unique prediction of the gas composition without imposing further assumptions. Despite this, non-injective gas sensor arrays could still be practically useful.

First, the response of a non-injective sensor array places potentially useful constraints on the gas composition. For example, consider the single HKUST-1 sensor in figure 5. The response under CH₄/CO₂/N₂ mixtures places tight bounds on the mole fraction of CO₂ in the mixture. On the other hand, the response under CH₄/CO₂/C₂H₆ mixtures cannot delineate between dominantly CH₄/CO₂ and CH₄/C₂H₆ mixtures (see figure 2). Nevertheless, the response *does* place

tight bounds on the *sum* of the CO_2 and C_2H_6 mole fractions and, hence, the CH_4 mole fraction (see figure 6). This tight bound on x_{CH_4} could be very useful and sufficient for certain applications.

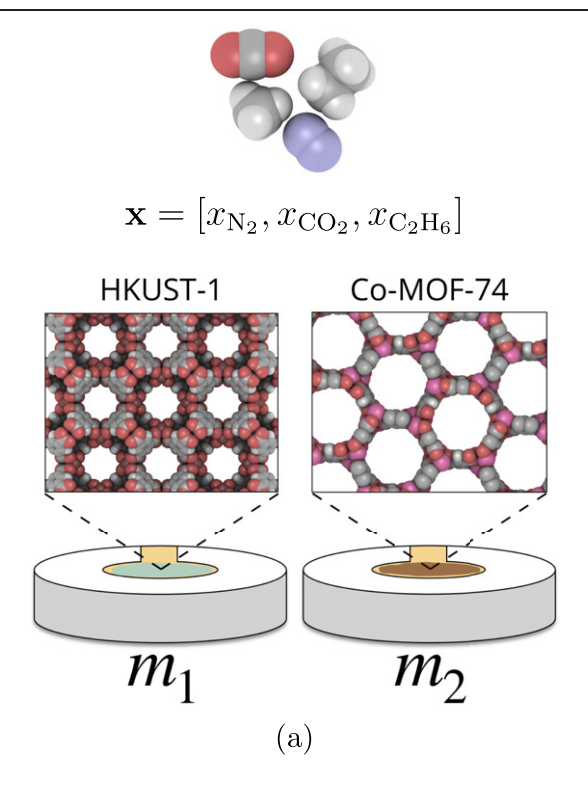
Second, imposing additional assumptions about the gas composition can grant the inverse problem a unique solution. Suppose the sensor response changed from \mathbf{m}_{op} , at the operating gas composition \mathbf{x}_{op} , to \mathbf{m}' . Invoking the linear approximation in equation (2), the inverse problem is to find \mathbf{x}' that satisfies:

$$\mathbf{J}(\mathbf{x}_{op})(\mathbf{x}' - \mathbf{x}_{op}) = \mathbf{m}' - \mathbf{m}_{op} =: \Delta \mathbf{m}. \tag{17}$$

Because $\mathbf{J}(\mathbf{x}_{op})$ is fat for a non-injective (M < G) gas sensor array, equation (17) has infinite solutions (fewer equations than unknowns). However, if we impose an additional assumption that the minimal-L2-norm gas composition change $\Delta \mathbf{x} := \mathbf{x}' - \mathbf{x}_{op}$ from \mathbf{x}_{op} is the culprit of the change in the sensor response $\Delta \mathbf{m}$, the inverse problem is granted a unique solution. The altered inverse problem:

$$\min_{\Delta \mathbf{x}: \ \mathbf{J}(\mathbf{x}_{op})\Delta \mathbf{x} = \Delta \mathbf{m}} \|\Delta \mathbf{x}\| \tag{18}$$

has a unique solution given by $\Delta \mathbf{x} = \mathbf{J}^{\dagger} \Delta \mathbf{m}$, with \mathbf{J}^{\dagger} the Moore–Penrose pseudo-inverse [63] of J. Again, the SVD in



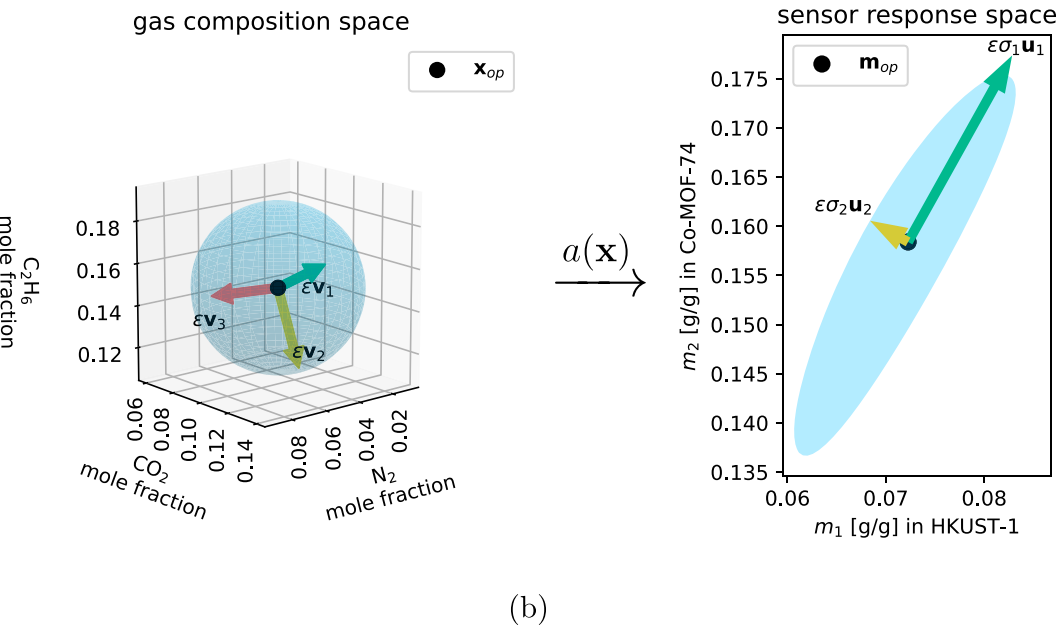


Figure 8. Case M=2, G=3: visualization of $a(\mathbf{x})$ and unresponsive directions for a two-MOF sensor array immersed in a CH₄/N₂/CO₂/C₂H₆ gas mixture at 1 bar and 298 K. (a) The two-MOF sensor array uses HKUST-1 and Co-MOF-74 as recognition elements. (b) The mapping from gas composition space (left) to sensor response space (right) under $a(\mathbf{x})$ for the sensor array in (a). The small sphere of radius $\epsilon=0.04$ in composition space (blue) is mapped to the solid ellipse-like shape (not an exact ellipse like in figure 3(b) because $a(\mathbf{x})$ is nonlinear) in response space (blue). Under the linear approximant of $a(\mathbf{x})$, $\tilde{a}(\mathbf{x})$, the vectors $\epsilon \mathbf{v}_2$, $\epsilon \mathbf{v}_3$ are mapped to $\epsilon \sigma_1 \mathbf{u}_1$, $\epsilon \sigma_2 \mathbf{u}_2$, $\mathbf{0}$, respectively. The unresponsive direction is \mathbf{v}_3 (red). The sensitive direction is \mathbf{v}_1 (green).

equation (6) plays the central role, as the pseudo-inverse can be constructed from it [63].

7. Conclusions and discussion

Mathematically, gas sensor arrays map each gas composition vector \mathbf{x} to an equilibrium response vector \mathbf{m} . For gravimetric, MOF-based gas sensor arrays, this mapping is characterized by a mixed-gas adsorption model $\mathbf{m} = a(\mathbf{x})$. An observation of the (total) mass of gas adsorbed in an MOF generally places one independent constraint $m_i = a_i(\mathbf{x})$ on the gas composition. We considered when there are fewer MOFs in the array than degrees of freedom in the gas composition (the number of components minus one, given fixed temperature and pressure). As a result, the mapping $a: \mathbf{x} \mapsto \mathbf{m}$ is non-injective (many-to-one). Then, some gas composition changes from \mathbf{x}_{op} to \mathbf{x}' do not cause changes in the sensor response \mathbf{m}_{op} despite $\mathbf{x}' \neq \mathbf{x}_{op}$ and thus are undetectable. We showed how to determine the local unresponsive subspace of gas composition space from the null space of the Jacobian matrix **J** of the adsorption model $a(\mathbf{x})$. Whereupon small changes in gas composition in an unresponsive direction, the sensor response remains constant. More, the right singular vectors of J associated with its non-zero singular values give directions in gas composition space to which the sensor is responsive, ranked by sensitivity. We demonstrated the identification of unresponsive and ranked responsive directions in non-injective, single- and double-MOF sensor arrays based on HKUST-1 and Co-MOF-74 immersed in a mixture involving CH₄, CO₂, C₂H₆, and N₂ relevant to natural gas sensing [50]. Our case studies involved ≤two MOFs and ≤four components in the gas, instructively allowing us to visualize $a(\mathbf{x})$ and clarify the meaning of the unresponsive and ranked responsive directions in gas composition space. The SVD in equation (6) is particularly powerful for large sensor arrays and high-dimensional gas composition spaces where visualization of $a(\mathbf{x})$ is extremely difficult.

Unsurprisingly, the identification of unresponsive and ranked responsive directions have analogies in multiple-input, multiple-output control systems: observability [73–75] and directionality [76, 77], respectively.

A limitation of our method to identify unresponsive directions in gas composition space is that it pertains to *small* changes in gas composition (via the Taylor expansion in equation (2); this approximation is illustrated in figure 8(b)).

Why is it useful to identify unresponsive directions in gas sensors? A gas sensor is unresponsive to and thus cannot detect gas composition changes in the unresponsive direction. Determining the unresponsive directions of a gas sensor is important to quantify its limitations and identify its vulnerabilities to adversarial attacks [49]. In addition, given a set of candidate non-injective gas sensors for a sensing task, we may be able rank their fitness according to their unresponsive directions e.g. having a minimal component along a pertinent direction.

Does the notion and identification of unresponsive directions generalize beyond gravimetric, MOF-based sensors? The notion and process of identifying unresponsive directions herein generalizes beyond the specific sensing mechanism of observing the total mass of adsorbed gas in an MOF. To adapt to a generic array of sensing elements, each exhibiting some observable property dependent on the gas composition, redefine:

- m as the vector containing the observed properties of the M sensing elements in response to the gas composition x.
- $a(\mathbf{x})$ as a function that models the response **m** to each gas composition **x**.

Even without much understanding of the underlying physics linking the response to the gas composition, we could build the model $a(\mathbf{x})$ as follows. Construct the sensor array. Conduct gas exposure experiments: observe the response over a grid of gas compositions to generate data $\mathcal{D} = \{(\mathbf{x}_i, \mathbf{m}_i)\}$. Build a regression model of $a(\mathbf{x})$ using the training data \mathcal{D} .

Gravimetric MOF sensors are attractive from a modeling perspective because we can construct a reasonable model $a(\mathbf{x})$ without actually constructing the sensor array and conducting laborious experiments. Gas adsorption data in MOFs is abundant; thermodynamic theories of gas adsorption are well-developed; and molecular models and simulations can predict adsorption in MOFs. The latter enables the computational design of MOF-based gas sensor arrays, as exemplified by Wilmer and co-workers [54, 55], who use molecular simulations of adsorption to predict the response of gravimetric, MOF-based sensor arrays and then evaluate their fitness for gas sensing.

How can we remedy non-injective gas sensors to give a determined inverse problem? The observed response of a non-injective gas sensor generally places an insufficient number of constraints on the gas composition to give the inverse problem a unique solution. We can make a non-injective sensor array injective by (i) retrofitting it with additional sensing elements (MOFs), (ii) designing sensing elements (MOFs) that do not respond appreciably to interferents in the gas that we are not concerned about, or (iii) imposing additional assumptions on the gas composition as in equation (18).

Is an injective sensor array the end goal? The inverse problem associated with an injective sensor array will theoretically always have a unique solution. However, in practice, the measurements of the masses of gas adsorbed in each MOF are corrupted by measurement error. As a result, the applied inverse problem [78] for an injective sensor array could still (i) have no solution or (ii) be ill-conditioned, where small measurement errors lead to large changes in the predicted gas composition [40]. The conditioning of the inverse problem, colloquially speaking, depends on the diversity of the MOFs in the array and their interactions with the components of the gas. One method to evaluate the fitness of different injective sensor arrays is to analyze the conditioning of their inverse problem [40].

Future work remains. First, we posed the gas sensing problem in terms of the *equilibrium* response of the gas sensor. However, the mass of gas adsorbed in an MOF is generally dynamic; gas must enter into and diffuse in the thin film of the MOF attached to the QCM [79–81]. Future work entails

(i) considering the diffusion kinetics when evaluating MOF-based sensors to avoid slow response times, (ii) posing inverse problems in terms of the dynamic response of the sensor, as in Rajagopalan and Petit [57], and (iii) extracting additional information about the gas composition from the dynamics of the response.

Second, we assumed isothermal conditions. We may wish to use a gas sensor to robustly predict the gas composition in a range of temperatures. Future work entails building an adsorption model $a(\mathbf{x}; T)$ that applies under different temperatures T, then (a) inputting a separate measurement of T or (b) determining T as part of the inverse problem.

Third, imposing additional assumptions on the gas composition can endow the underdetermined inverse problem associated with a non-injective gas sensor with a unique solution. This idea of imposing additional assumptions, consistent with but not imposed by the physics underlying the problem, is a common approach to, given an inverse problem with many solutions, grant it a unique solution [78]. We provided one example in equation (18), where we sought the minimum-norm change in the gas composition consistent with the change in the response.

Fourth, for MOF-based gas sensor arrays to operate in practical conditions, we need to engineer MOFs that are (1) thermally, mechanically, and chemically stable [13, 82] and (2) hydrophobic, for applications where moisture is present, so that the response is not dominated by water adsorption [14, 83, 84].

Acknowledgments

We acknowledge support from the U.S. Department of Defense (DoD) Defense Threat Reduction Agency (HDTRA-19-31270) (NG, CMS, PT) and the National Science Foundation (NSF) (Award 1920945) (AH, CMS, XF).

Data availability statement

The data and Python code to reproduce this study are openly available at the following URL: https://github.com/SimonEnsemble/unresponsive_directions_in_sensors.

ORCID iDs

E Adrian Henle https://orcid.org/0000-0002-3331-7173 Cory M Simon https://orcid.org/0000-0002-8181-9178

References

- [1] Hu W et al 2018 Electronic noses: from advanced materials to sensors aided with data processing Adv. Mater. Technol. 4
- [2] Kumar P, Morawska L, Martani C, Biskos G, Neophytou M, Di Sabatino S, Bell M, Norford L and Britter R 2015 The rise of low-cost sensing for managing air pollution in cities *Environ. Int.* 75 199–205

- [3] Konvalina G and Haick H 2014 Sensors for breath testing: from nanomaterials to comprehensive disease detection Acc. Chem. Res. 47 66–76
- [4] Yousefi H, Su H-M, Imani S M, Alkhaldi K, Filipe C D and Didar T F 2019 Intelligent food packaging: a review of smart sensing technologies for monitoring food quality ACS Sens. 4 808–21
- [5] Islamoglu T, Chen Z, Wasson M C, Buru C T, Kirlikovali K O, Afrin U, Mian M R and Farha O K 2020 Metal-organic frameworks against toxic chemicals *Chem. Rev.* 120 8130–60
- [6] Vemuri R S and Paul A 2015 An overview of detection and neutralization of chemical warfare agents using metal organic frameworks J. Bioterrorism Biodef. 6 1000137
- [7] Wilson A 2013 Diverse applications of electronic-nose technologies in agriculture and forestry Sensors 13 2295–348
- [8] Furukawa H, Cordova K E, O'Keeffe M and Yaghi O M 2013 The chemistry and applications of metal-organic frameworks Science 341 1230444
- [9] Kreno L E, Leong K, Farha O K, Allendorf M, Van Duyne R P and Hupp J T 2011 Metal-organic framework materials as chemical sensors *Chem. Rev.* 112 1105–25
- [10] Wales D J, Grand J, Ting V P, Burke R D, Edler K J, Bowen C R, Mintova S and Burrows A D 2015 Gas sensing using porous materials for automotive applications *Chem. Soc. Rev.* 44 4290–321
- [11] Li H-Y, Zhao S-N, Zang S-Q and Li J 2020 Functional metalorganic frameworks as effective sensors of gases and volatile compounds *Chem. Soc. Rev.* 49 6364–401
- [12] Small L J, Schindelholz M E and Nenoff T M 2021 Hold on tight: MOF-based irreversible gas sensors *Ind. Eng. Chem. Res.* 60 7998–8006
- [13] Howarth A J, Liu Y, Peng L, Li Z, Wang T C, Hupp J T and Farha O K 2016 Chemical, thermal and mechanical stabilities of metal-organic frameworks *Nat. Rev. Mater.* 1 15018
- [14] Ding M, Cai X and Jiang H-L 2019 Improving MOF stability: approaches and applications *Chem. Sci.* **10** 10209–30
- [15] Tchalala M R et al 2019 Fluorinated MOF platform for selective removal and sensing of SO₂ from flue gas and air Nat. Commun. 10 1328
- [16] Campbell M G, Liu S F, Swager T M and Dincă M 2015 Chemiresistive sensor arrays from conductive 2D metalorganic frameworks J. Am. Chem. Soc. 137 13780–3
- [17] Meng Z, Aykanat A and Mirica K A 2018 Welding metallophthalocyanines into bimetallic molecular meshes for ultrasensitive, low-power chemiresistive detection of gases *J. Am. Chem. Soc.* 141 2046–53
- [18] Feng Y, Wang Y and Ying Y 2021 Structural design of metalorganic frameworks with tunable colorimetric responses for visual sensing applications *Coord. Chem. Rev.* 446 214102
- [19] Lin R B, Liu S Y, Ye J W, Li X Y and Zhang J P 2016 Photoluminescent metal-organic frameworks for gas sensing Adv. Sci. 3 1500434
- [20] Lustig W P, Mukherjee S, Rudd N D, Desai A V, Li J and Ghosh S K 2017 Metal-organic frameworks: functional luminescent and photonic materials for sensing applications *Chem. Soc. Rev.* 46 3242–85
- [21] Allendorf M D, Houk R J T, Andruszkiewicz L, Talin A A, Pikarsky J, Choudhury A, Gall K A and Hesketh P J 2008 Stress-induced chemical detection using flexible metalorganic frameworks J. Am. Chem. Soc. 130 14404–5
- [22] Yeung H H-M, Yoshikawa G, Minami K and Shiba K 2020 Strain-based chemical sensing using metal-organic framework nanoparticles J. Mater. Chem. A 8 18007–14
- [23] Shekhah O, Liu J, Fischer R A and Wöll C 2011 MOF thin films: existing and future applications *Chem. Soc. Rev.* 40 1081–106
- [24] Stassen I, Burtch N, Talin A, Falcaro P, Allendorf M and Ameloot R 2017 An updated roadmap for the integration

- of metal-organic frameworks with electronic devices and chemical sensors *Chem. Soc. Rev.* **46** 3185–241
- [25] Semrau A L, Zhou Z, Mukherjee S, Tu M, Li W and Fischer R A 2021 Surface-mounted metal-organic frameworks: past, present, and future perspectives *Langmuir* 37 6847–63
- [26] Yamagiwa H, Sato S, Fukawa T, Ikehara T, Maeda R, Mihara T and Kimura M 2014 Detection of volatile organic compounds by weight-detectable sensors coated with metalorganic frameworks Sci. Rep. 4 6247
- [27] Tu M, Wannapaiboon S, Khaletskaya K and Fischer R A 2015 Engineering zeolitic-imidazolate framework (ZIF) thin film devices for selective detection of volatile organic compounds Adv. Funct. Mater. 25 4470–9
- [28] Tchalala M R, Belmabkhout Y, Adil K, Chappanda K N, Cadiau A, Bhatt P M, Salama K N and Eddaoudi M 2018 Concurrent sensing of CO₂ and H₂O from air using ultramicroporous fluorinated metal-organic frameworks: effect of transduction mechanism on the sensing performance ACS Appl. Mater. Interfaces 11 1706–12
- [29] Okur S, Qin P, Chandresh A, Li C, Zhang Z, Lemmer U and Heinke L 2020 An enantioselective e-nose: an array of nanoporous homochiral MOF films for stereospecific sensing of chiral odors Angew. Chem., Int. Ed. 60 3566–71
- [30] Okur S et al 2021 Sniff species: SURMOF-based sensor array discriminates aromatic plants beyond the genus Level Chemosensors 9 171
- [31] Kim K-J, Culp J T, Ohodnicki P R, Thallapally P K and Tao J 2021 Synthesis of high-quality mg-MOF-74 thin films via vapor-assisted crystallization ACS Appl. Mater. Interfaces 13 35223-31
- [32] Audu C O, Chen D, Kung C-W, Snurr R Q, Nguyen S B T, Farha O K and Hupp J T 2021 Transport diffusion of linear alkanes (C₅-C₁₆) through thin films of ZIF-8 as assessed by quartz crystal microgravimetry *Langmuir* **37** 9405–14
- [33] Stavila V et al 2016 Thin film growth of nbo MOFs and their integration with electroacoustic devices Adv. Funct. Mater. 26 1699–707
- [34] Paschke B, Wixforth A, Denysenko D and Volkmer D 2017 Fast surface acoustic wave-based sensors to investigate the kinetics of gas uptake in ultra-microporous frameworks *ACS Sens*. **2** 740–7
- [35] Devkota J, Kim K-J, Ohodnicki P R, Culp J T, Greve D W and Lekse J W 2018 Zeolitic imidazolate framework-coated acoustic sensors for room temperature detection of carbon dioxide and methane *Nanoscale* 10 8075–87
- [36] Olorunyomi J F, Geh S T, Caruso R A and Doherty C M 2021 Metal-organic frameworks for chemical sensing devices *Mater. Horiz.*
- [37] Chui S S, Lo S M-F, Charmant J P H, Orpen A G and Williams I D 1999 A chemically functionalizable nanoporous material [Cu₃(TMA)₂(H₂O)₃]_n Science **283** 1148–50
- [38] Wang L 2020 Metal-organic frameworks for QCM-based gas sensors: a review Sensors Actuators A 307 111984
- [39] Liu X, Cheng S, Liu H, Hu S, Zhang D and Ning H 2012 A survey on gas sensing technology Sensors 12 9635–65
- [40] Sousa R and Simon C M 2020 Evaluating the fitness of combinations of adsorbents for quantitative gas sensor arrays ACS Sens. 5 4035–47
- [41] Sturluson A, Sousa R, Zhang Y, Huynh M T, Laird C, York A H P, Silsby C, Chang C-H and Simon C M 2020 Curating metal-organic frameworks to compose robust gas sensor arrays in dilute conditions ACS Appl. Mater. Interfaces 12 6546–64
- [42] Hu W et al 2019 Electronic noses: from advanced materials to sensors aided with data processing Adv. Mater. Technol. 4 1800488
- [43] Albert K J, Lewis N S, Schauer C L, Sotzing G A, Stitzel S E, Vaid T P and Walt D R 2000 Cross-reactive chemical sensor arrays Chem. Rev. 100 2595–626

- [44] Gardner J W and Bartlett P N 1994 A brief history of electronic noses *Sensors Actuators* B **18** 210–1
- [45] Jurs P C, Bakken G A and McClelland H E 2000 Computational methods for the analysis of chemical sensor array data from volatile analytes *Chem. Rev.* 100 2649–78
- [46] Okur S, Zhang Z, Sarheed M, Nick P, Lemmer U and Heinke L 2020 Towards a MOF e-nose: a SURMOF sensor array for detection and discrimination of plant oil scents and their mixtures Sensors Actuators B 306 127502
- [47] Lee T, Liu Z X and Lee H L 2011 A biomimetic nose by microcrystals and oriented films of luminescent porous metalorganic frameworks Cryst. Growth Des. 11 4146–54
- [48] Ko M, Aykanat A, Smith M and Mirica K 2017 Drawing sensors with ball-milled blends of metal-organic frameworks and graphite Sensors 17 2192
- [49] Biggio B and Roli F 2018 Wild patterns: ten years after the rise of adversarial machine learning *Pattern Recognit.* **84** 317–31
- [50] Faramawy S, Zaki T and Sakr A A-E 2016 Natural gas origin, composition, and processing: a review J. Nat. Gas Sci. Eng. 34 34–54
- [51] Myers A L and Prausnitz J M 1965 Thermodynamics of mixedgas adsorption AIChE J. 11 121–7
- [52] Walton K S and Sholl D S 2015 Predicting multicomponent adsorption: 50 years of the ideal adsorbed solution theory AIChE J. 61 2757–62
- [53] Gustafson J A and Wilmer C E 2019 Intelligent selection of metal-organic framework arrays for methane sensing via genetic algorithms ACS Sens. 4 1586–93
- [54] Gustafson J A and Wilmer C E 2017 Computational design of metal-organic framework arrays for gas sensing: influence of array size and composition on sensor performance *J. Phys. Chem.* C 121 6033–8
- [55] Gustafson J A and Wilmer C E 2018 Optimizing information content in MOF sensor arrays for analyzing methane-air mixtures Sensors Actuators B 267 483–93
- [56] Day B A and Wilmer C E 2020 Genetic algorithm design of MOF-based gas sensor arrays for CO₂-in-air sensing *Sensors* 20 924
- [57] Rajagopalan A K and Petit C 2021 Material screening for gas sensing using an electronic nose: gas sorption thermodynamic and kinetic considerations 10.26434/chemrxiv.14578497.v1 (accessed 23 August 2021) (ChemRxiv)
- [58] Pearce T C 2000 Odor to sensor space transformations in biological and artificial noses *Neurocomputing* 32–33 941–52
- [59] Swenson H and Stadie N P 2019 Langmuir's theory of adsorption: a centennial review *Langmuir* 35 5409–26
- [60] Sturluson A et al 2019 The role of molecular modelling and simulation in the discovery and deployment of metal-organic frameworks for gas storage and separation Mol. Simul. 45 1082–121
- [61] Dubbeldam D, Torres-Knoop A and Walton K S 2013 On the inner workings of Monte Carlo codes Mol. Simul. 39 1253–92
- [62] Kalman D 1996 A singularly valuable decomposition: the SVD of a matrix Coll. Math. J. 27 2–23
- [63] Strang G 2016 Introduction to Linear Algebra vol 5 (Wellesley, MA: Wellesley-Cambridge Press)
- [64] Dietzel P D C, Morita Y, Blom R and Fjellvåg H 2005 An in situ high-temperature single-crystal investigation of a dehydrated metal-organic framework compound and field-induced magnetization of one-dimensional metal-oxygen chains Angew. Chem., Int. Ed. 44 6354–8
- [65] Hendon C H and Walsh A 2015 Chemical principles underpinning the performance of the metal-organic framework HKUST-1 Chem. Sci. 6 3674–83
- [66] Dietzel P D C, Besikiotis V and Blom R 2009 Application of metal-organic frameworks with coordinatively unsaturated metal sites in storage and separation of methane and carbon dioxide J. Mater. Chem. 19 7362

- [67] Mason J A, Veenstra M and Long J R 2014 Evaluating metalorganic frameworks for natural gas storage *Chem. Sci.* 5 32–51
- [68] Millward A R and Yaghi O M 2005 Metal-organic frameworks with exceptionally high capacity for storage of carbon dioxide at room temperature J. Am. Chem. Soc. 127 17998–9
- [69] He Y, Krishna R and Chen B 2012 Metal-organic frameworks with potential for energy-efficient adsorptive separation of light hydrocarbons *Energy Environ. Sci.* 5 9107
- [70] Rother J and Fieback T 2013 Multicomponent adsorption measurements on activated carbon, zeolite molecular sieve and metal-organic framework Adsorption 19 1065–74
- [71] Yu D, Yazaydin A O, Lane J R, Dietzel P D C and Snurr R Q 2013 A combined experimental and quantum chemical study of CO₂ adsorption in the metal-organic framework CPO-27 with different metals *Chem. Sci.* 4 3544
- [72] Simon C M, Smit B and Haranczyk M 2016 pyIAST: ideal adsorbed solution theory (IAST) Python package *Comput. Phys. Commun.* 200 364–80
- [73] Castillo E, Conejo A J, Pruneda R E and Solares C 2005 State estimation observability based on the null space of the measurement Jacobian matrix *IEEE Trans. Power Syst.* 20 1656–8
- [74] Liu Y-Y, Slotine J-J and Barabasi A-L 2013 Observability of complex systems Proc. Natl. Acad. Sci. 110 2460-5
- [75] Gilbert E G 1963 Controllability and observability in multivariable control systems *J. Soc. Ind. Appl. Math.* A 1 128–51

- [76] Skogestad S and Postlethwaite I 2007 Multivariable Feedback Control: Analysis and Design vol 2 (Chichester: Wiley)
- [77] Weisberg Andersen H and Kümmel M 1992 Evaluating estimation of gain directionality J. Process Control 2 59–66
- [78] Sabatier P C 2000 Past and future of inverse problems J. Math. Phys. 41 4082–124
- [79] Heinke L and Wöll C 2013 Adsorption and diffusion in thin films of nanoporous metal-organic frameworks: ferrocene in SURMOF Cu₂(ndc)₂(dabco) *Phys. Chem. Chem. Phys.* 15 9295–9
- [80] Heinke L, Gu Z and Wöll C 2014 The surface barrier phenomenon at the loading of metal-organic frameworks *Nat. Commun.* 5 4562
- [81] Tobias T, Lauerer A, Heinke L, Chmelik C, Zimmermann N E R, Keil F J, Ruthven D M and Kärger J 2015 Transport in nanoporous materials including MOFs: the applicability of Fick's laws Angew. Chem., Int. Ed. 54 14580-3
- [82] Low J J, Benin A I, Jakubczak P, Abrahamian J F, Faheem S A and Willis R R 2009 Virtual high throughput screening confirmed experimentally: porous coordination polymer hydration J. Am. Chem. Soc. 131 15834–42
- [83] Canivet J, Bonnefoy J, Daniel C, Legrand A, Coasne B and Farrusseng D 2014 Structure-property relationships of water adsorption in metal-organic frameworks *New J. Chem.* 38 3102–11
- [84] Jayaramulu K, Geyer F, Schneemann A, KmenS, Otyepka M, Zboril R, Vollmer D and Fischer R A 2019 Hydrophobic metal-organic frameworks Adv. Mater. 31 1900820